Top-down and bottom-up approaches to transparent, flexible and luminescent nitrogen-doped carbon nanodot-clay hybrid films

Dimos, Konstantinos; Arcudi, Francesca; Kouloumpis, Antonios; Koutselas, Ioannis B.; Rudolf, Petra; Prato, Maurizio

Published in:
Nanoscale

DOI:
10.1039/c7nr02673k

Publication date:
2017

Nanoscale

PAPER

View Article Online
View Journal | View Issue

Cite this: *Nanoscale*, 2017, **9**, 10256

Top-down and bottom-up approaches to transparent, flexible and luminescent nitrogen-doped carbon nanodot-clay hybrid films†

Konstantinos Dimos, *‡[a,b] Francesca Arcudi, *‡[c] Antonios Kouloumpis, [a,d] Ioannis B. Koutselas, [e] Petra Rudolf, [d] Dimitrios Gournis *[a] and Maurizio Prato *[c,f,g]

Received 14th April 2017,
Accepted 20th June 2017

DOI: 10.1039/c7nr02673k

rsc.li/nanoscale

Two easy approaches are successfully employed for the preparation of nitrogen-doped carbon nanodot (NCND)-clay hybrids (bulk solids and thin films). Fluorescent and small NCNDs are intercalated within the interlayer space of LAPONITE® clay with a simple ion exchange reaction in bulk or embedded between functionalized LAPONITE® sheets by combining a layer-by-layer approach with a self-assembly process. In both cases, homogeneous hybrids with 2D-ordered NCNDs (accounting for >20 wt%) are produced, with the NCND optoelectronic properties preserved. Drop casting of suspensions or self-assembly on flexible substrates allows the fabrication of luminescent flexible films. The transparency of the films is found to be adjustable either by controlling the concentration of the drop-cast suspensions or by the number of layers in the self-assembly procedure. The prepared films are stable over time: the inert LAPONITE® platelets not only guide the highly ordered 2D assemblies of NCNDs in the interlayer space but also protect them from external agents, which could affect their surfaces and thus alter their optoelectronic properties.

Introduction

Carbon nanodots (CNDs) are an emergent class of carbon nanomaterials that include quasispherical nanoparticles with sizes below 10 nm.[1] Since their discovery,[2] CNDs have attracted a lot of attention, since they combine unique and attractive characteristics, such as tunable photoluminescence, low toxicity, biocompatibility and low photobleaching.[3,4] As a result, CNDs could possibly lead to breakthroughs in biosensing, bioimaging and nanomedicine, eventually outperforming conventional toxic metal-based quantum dots.[5] Moreover, CNDs show promise in areas such as light emitting diodes, solar cells, sensing, catalysis, and photovoltaic devices,[6–8] while engineering their surface functionality may expand their applicability.[9–12]

On the other hand, in another exciting field of nanotechnology, the availability of two-dimensional (2D) structures, such as graphene, transition metal dichalcogenides or more recently phosphorene, has catalyzed the interest in layered materials.[13] Quantum confinement within the extended planar network where electrons can travel endows these materials with extraordinary properties. Conventional semiconducting nanoparticles have been combined with 2D hosts such as clay minerals in order to create sophisticated homogeneous, 2D-ordered hybrids, in the form of small aggregates or extended thin films, which maintain the optoelectronic properties of the quantum dots.[14,15] Recently, engineered systems of functional CND-based hybrids have begun to emerge. CNDs have been grafted to fibers to form hybrids with clays for LEDs,[16] supported on layered double hydroxides to act as catalysts,[17] or integrated into silica[18,19] or polymer-assisted luminescent composite films.[20–23]

However, to the best of our knowledge, no highly ordered arrays in which CNDs are intercalated in 2D matrices have been reported so far. Ideal hosts for such purposes are clay minerals and especially the members of the smectite group. These phyllomorphous silicates possess exceptional swelling, adsorption, ion exchange and intercalation properties along with high surface areas.[24] Hence, smectites are a highly suitable candidate for hosting CNDs in their interlayer space.

[a]Department of Materials Science & Engineering, University of Ioannina, GR-45110 Ioannina, Greece. E-mail: kdimos@cc.uoi.gr, dgourni@cc.uoi.gr
[b]Cambridge Graphene Centre, University of Cambridge, Cambridge CB3 0FA, UK
[c]Centre of Excellence for Nanostructured Materials (CENMAT), INSTM, unit of Trieste, Department of Chemical and Pharmaceutical Sciences, University of Trieste, via L. Giorgieri 1, 34127 Trieste, Italy. E-mail: francescarcudi@gmail.com, prato@units.it
[d]Zernike Institute for Advanced Materials, University of Groningen, Nijenborgh 4, NL-9747 AG Groningen, The Netherlands
[e]Department of Materials Science, University of Patras, GR-26504 Patras, Greece
[f]CIC BiomaGUNE, Parque Tecnológico de San Sebastián, Paseo Miramón, 182, 20009 San Sebastián (Guipúzcoa), Spain
[g]Basque Foundation for Science, Ikerbasque, Bilbao 48013, Spain

†Electronic supplementary information (ESI) available: Fig. S1–S6 and Scheme S1. See DOI: 10.1039/c7nr02673k

‡These authors contributed equally.

Recently, we reported a simple bottom-up approach to bright fluorescent nitrogen-doped CNDs (NCNDs) using a microwave reactor.[25] These NCNDs have excellent solubility in water and abundant nitrogen- and oxygen-bearing functional groups on their surface, which should allow ion-exchange-driven intercalation within the clay interlayer space.

In this paper, we describe the intercalation of our NCNDs in synthetic LAPONITE® (Lap, LAPONITE® is a registered trademark by BYK Additives Ltd) producing luminescent hybrids, and the fabrication of transparent and flexible thin films based on these hybrids. Two diverse approaches were employed for the formation of hybrids and thin films; a top-down approach producing bulk composites and films by subsequent drop casting from suspensions, and a bottom-up layer-by-layer (LbL) approach yielding ultra-thin hybrid films. The first approach uses bulk pristine materials and leads to hybrids with the desired nanostructure, while the second relies on the Langmuir–Schaefer (LS) and self-assembly (SA) techniques to build up multilayered films in a controllable fashion. The final materials exhibit a high NCND content (above 20 wt%) and are homogeneous, while their transparency can be easily tuned.

Experimental

Sample preparation

Nitrogen-doped carbon nanodots (NCNDs) were synthesized and characterized as described in detail elsewhere.[25] In brief, NCNDs were obtained *via* microwave irradiation of an aqueous solution of L-arginine and ethylenediamine (EDA) (1 : 1 mol/mol). Typically, L-arginine (87.0 mg), EDA (33.0 μL) and Milli-Q water (100.0 μL) were heated to 240 °C, at 26 bar and 200 W for 180 s. Upon microwave heating the solution became brown as a result of NCND formation. The solution was diluted with water and filtered through a 0.1 μm microporous membrane separating a deep yellow solution that was dialyzed against pure water through a dialysis membrane for 2 days. Finally, the aqueous solution of NCNDs was lyophilized, yielding a brownish solid.

For the top-down synthesis of the NCND-Lap hybrid, 100 mg of LAPONITE® (from The Clay Minerals Society, chemical formula: $Na_{0.56}[Mg_{5.4}Li_{0.4}]Si_8O_{20}(OH)_4$) were fully exfoliated upon stirring for 24 h in 400 mL ultrapure water (Milli-Q); then 1.5 mL of an aqueous (Milli-Q) solution containing 75 mg NCNDs were added and stirring was continued for an additional 24 h. The final product (NCNDs-Lap) was isolated by centrifugation. Flexible NCND-Lap films on a PET transparent substrate were fabricated by drop casting aliquots of a NCNDs-Lap aqueous suspension.

For the bottom-up approach first a Langmuir–Blodgett trough (KSV 2000 Nima Technology model) was cleaned with ethanol and water. LAPONITE® suspensions in ultrapure water (0.02 mg mL^{-1}) were used as the subphase and a Pt Wilhelmy plate was employed to monitor the surface pressure. For the formation of a LAPONITE®-containing Langmuir film at the air–water interface we followed a similar procedure to that reported in ref. 26: 50 μL of a 0.2 mg mL^{-1} dimethyldioctadecylammonium bromide (DODA) solution in chloroform/methanol 9/1 (v/v) was spread onto the subphase with the help of a microsyringe. After a waiting time of 15 min, the hybrid DODA-LAPONITE® layer was compressed at a rate of 5 mm min^{-1} until the target surface pressure of 20 mN m^{-1} was reached, forming a dense DODA-LAPONITE® Langmuir film. This pressure was maintained constant throughout the deposition process. Layers were transferred onto the hydrophobic quartz substrates (prepared as described in the ESI, Scheme S1†) by the Langmuir Schaefer technique (horizontal dipping), with downward and lifting speeds of 10 and 5 mm min^{-1}, respectively. After the transfer of the DODA-LAPONITE® layer to substrates, the surface of the transferred film was rinsed with pure water several times and dried with a flow of N_2 gas. The hybrid LAPONITE® film was dipped into an aqueous solution of NCNDs (0.2 mg mL^{-1}) to induce the formation of a LAPONITE®-NCND hybrid by the self-assembly and rinsed again several times by dipping into ultrapure water and dried with nitrogen flow. A hybrid multilayer film was formed by repeating this procedure (DODA-Lap-NCNDs), as shown in Fig. 5a. Pressure area (Π–a) isotherms of DODA monolayers in pure water and in LAPONITE® dispersion are shown in Fig. S4.†[27,28]

Analytical measurements

The θ–2θ X-ray powder diffraction data (XRD) were collected with a D8 Advance Bruker diffractometer using Cu Kα radiation (40 kV, 40 mA, λ = 1.54178 Å). Diffraction patterns were collected in the 2θ range from 1° to 25°, in steps of 0.02° and 2 s counting time per step. Thermogravimetric analysis (TGA) and differential thermal analysis (DTA) were performed using a PerkinElmer Pyris Diamond TG/DTA instrument. Samples of approximately 3–3.5 mg were heated in still air from 15 °C to 800 °C, with a heating rate of 5 °C min^{-1}. For recording Fourier transform infrared spectra on a PerkinElmer GX Fourier transform spectrometer in the frequency range of 400–4000 cm^{-1}, pellets of pulverized samples dispersed in KBr were used. The reported spectra are an average of 64 scans collected with 2 cm^{-1} resolution.

X-ray photoelectron spectroscopy (XPS) measurements were performed at a base pressure of 5×10^{-10} mbar in a SPECS GmbH instrument equipped with a monochromatic Mg Kα source ($h\nu$ = 1253.6 eV) and a Phoibos-100 hemispherical analyzer. The energy resolution was set to 0.3 eV and the photoelectron take-off angle was 45° with respect to the surface normal. All binding energies are reported ± 0.05 eV and referenced to the Si 2p at 99.15 eV. Spectral analysis included a Shirley background subtraction and peak deconvolution employing mixed Gaussian–Lorentzian functions, in a least squares curve-fitting program (WinSpec) developed at the Laboratoire Interdisciplinaire de Spectroscopie Electronique, University of Namur, Belgium. All measurements were carried out on freshly prepared samples. Four different spots were measured on each surface to check for reproducibility.

UV-Vis spectra were recorded on a Shimadzu UV-2401PC two beam spectrophotometer in the range of 200–800 nm, at a step of 0.5 nm, using a combination of deuterium and halogen lamps as sources. Photoluminescence emission and excitation (PL/PLE) spectra were recorded on a Jobin Yvon Fluorolog 3 spectrofluorometer FL-11 employing a 450 W Xenon lamp and a P928P photodetector; the slits were set at 5 nm. The PL/PLE spectra were corrected by the instrument-specific files supplied by the manufacturer, based on the measurements of compounds with known quantum yield, whereas emission peaks originating by water Raman scattering have been eliminated from the PL spectra. All optical UV-Vis and PL/PLE spectra of NCNDs-Lap suspensions placed in 10 mm path-length quartz cuvettes and of the NCNDs-Lap thin film deposited on quartz substrates were recorded at room temperature. For PL/PLE spectra, the detector-source geometry was at 90° with respect to the sample and for the PL/PLE measurements of the thin film the quartz substrate was placed in reflective geometry.

Results and discussion

Top-down approach

Nitrogen-doped carbon nanodots (NCNDs) were synthesized and characterized as described elsewhere.[25] 100 mg LAPONITE® were fully exfoliated upon stirring for 24 h in 400 mL ultrapure water (Milli-Q). Then 1.5 mL of an aqueous (Milli-Q) solution containing 75 mg NCNDs was added, while stirring was continued for an additional 24 h (Fig. 1a). The final product (NCNDs-Lap) was isolated by centrifugation. Flexible NCNDs-Lap films on a PET transparent substrate were fabricated by drop casting aliquots of a NCNDs-Lap aqueous suspension.

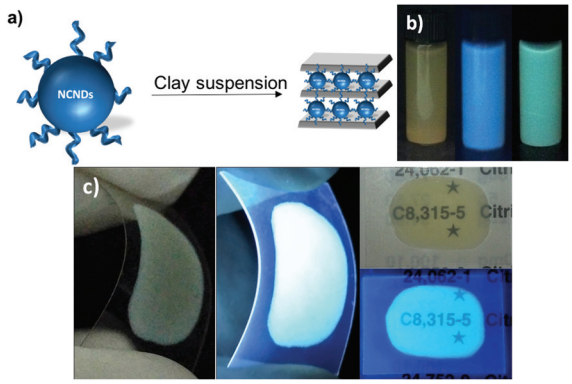

Fig. 1 (a) Schematic illustration of the NCNDs-Lap hybrid preparation; (b) digital photographs of a NCNDs-Lap aqueous suspension (2.5 mg mL^{-1}) with room lights on (left), with room lights on and UV (365 nm) illumination (center) and with room lights off (darkness) and UV (365 nm) illumination (right); (c) digital photographs of a transparent flexible NCNDs-Lap film deposited on a PET transparent substrate by drop casting aliquots of a NCNDs-Lap aqueous suspension with lights on (left and top right), and lights off and UV (365 nm) illumination (center and bottom right).

The fluorescence of NCNDs is preserved in the NCNDs-Lap aqueous suspension (Fig. 1b) and the NCNDs-Lap hybrid drop-cast onto a PET substrate from the aqueous suspension results in flexible, transparent and luminescent films (Fig. 1c).

Remarkably, luminescence and transparency are unique features of CNDs that are difficult to achieve with other carbon-based hybrids. The drop-casting method allows us to adjust these properties by controlling the concentration of the drop-cast suspensions and/or the total drop-cast volume.

The successful introduction of the NCNDs in the layered matrices was proven by X-ray powder diffraction (XRD). The XRD patterns of the pristine Lap and of NCNDs-Lap hybrid are shown in Fig. 2a. Both are typical of layered materials as they exhibit strong reflection peaks at $2\theta \sim 6.9°$ and ~4.6°, respectively, that originate from the (001) lattice planes. By employing Bragg's law, the corresponding d_{001} spacings can be calculated to be 12.8 ± 0.3 Å for Lap and 19.3 ± 0.3 Å for NCNDs-Lap. The significantly larger value of d_{001} for NCNDs-Lap testifies the successful intercalation of the NCNDs in the interlayer space of Lap. In fact, Lap is a smectite clay, also called a 2 : 1 clay, meaning that its platelets consist of an octahedral alumina layer sandwiched between two tetrahedral layers of silicon oxide (SiO_4) and are 9.6 Å thick.[29] Thus, the interlayer space of pristine Lap is (12.8–9.6) ≈ 3 Å and suggests the presence of a monolayer by water molecules; the interlamellar space of NCNDs-Lap is instead (19.3–9.6) ≈ 10 Å, which implies that small NCNDs of a size of ≈1 nm are intercalated between the LAPONITE® sheets.[30]

To estimate the amount of NCNDs incorporated in Lap, thermogravimetric (TGA), differential thermogravimetric (DTG) and differential thermal (DT) analyses were performed on the hybrid (Fig. 2b) as well as on the pristine Lap. The small weight loss below 100 °C with a corresponding endothermic peak is attributed to the removal of physisorbed water molecules. At higher temperatures and more specifically in the temperature region of 150–650 °C, which is marked with two vertical dashed lines, two broad exothermic peaks centered at ~346 °C and ~520 °C are observed; the related mass loss occurs mainly during these two exothermic reactions as better exposed by the DTG signal and amounts to 26%. The first

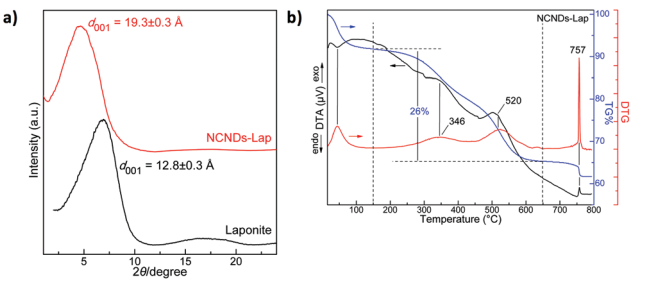

Fig. 2 (a) X-ray powder diffraction patterns of LAPONITE® and of the NCNDs-Lap hybrid prepared using the top-down approach; (b) thermogravimetric (TG), differential thermogravimetric (DTG) and differential thermal (DT) analysis curves of the NCNDs-Lap hybrid prepared with the top-down approach (bottom panel).

reaction probably corresponds to the decomposition of the functional groups present on the NCND surface, whereas the second reaction is the combustion of the remaining carbon, namely the core of the NCNDs. Above 650 °C the sample displays a narrow exothermic peak at 757 °C with a sharp but small weight loss, which is ascribed to the phase transition of LAPONITE® due to its dehydroxylation and crystallization of enstatite.[31] The relevant thermal analysis curves of pristine LAPONITE® are shown in Fig. S1 of the ESI,† where as expected the weight loss in the 150–650 °C temperature region typical of the combustion of carbon materials is minute (4%), no peaks are observed in the DTA and DTG signals and just a slight slope of the TGA signal is seen. Therefore, the NCND content in the NCNDs-Lap hybrid is estimated to be at least 22 wt% and could reach as much as 25–26 wt% in the case where the possible organic contaminants of Lap were completely removed during the preparation of the hybrid and the ion exchange reactions with the NCNDs. These percentages are consistent with the energy-dispersive X-ray analysis of a NCNDs-Lap flake (Fig. S2 of the ESI†).

The surface components of the NCNDs-Lap hybrid were determined by Fourier transform infrared (FT-IR) and X-ray photoelectron (XPS) spectroscopy methods (Fig. 3). The FT-IR spectrum displays peaks at 443, 651, 1009 and 3695 cm^{-1} originating from Lap, which can be assigned to the rocking vibration of Si–O–Si, the bending vibration of Mg–O–Si, the stretching vibration of Si–O–Si and the stretching vibration of O–H bonds from lattice hydroxyl groups, respectively.[15] The broad band centered at 3409 cm^{-1} and most of the intensity of the 1650 cm^{-1} peak are correlated with physisorbed water and specifically with the H_2O stretching and bending vibrations, respectively. The remaining bands are associated with the NCNDs, with oxygen and nitrogen surface functional groups.[25] In detail, the peak at 1361 cm^{-1} is related to the stretching vibration of C–O bonds, the one at 1457 cm^{-1} to the stretching vibration of C–N and/or bending of C–H bonds, while the 1559 cm^{-1} peak originates from the stretching of C═N and/or N–H bending. The 1709 cm^{-1} band is correlated with the stretching of C═O bonds from carboxyl groups, whereas the peaks at 2871 and 2953 cm^{-1} derive from the symmetric and asymmetric stretching vibrations of C–H bonds. In addition, stretching of C═C bonds or C═O bonds of carbonyl groups may contribute to the 1650 cm^{-1} band, while the stretching vibrations of O–H and N–H bonds from NCNDs contribute to the 3409 cm^{-1} band of water.[25]

XPS analysis confirms the above results since carbon, nitrogen, oxygen, silicon and magnesium are detected in the survey spectrum (not shown) and the signature of all the carbon-containing functional groups identified in the FT-IR analysis is found upon deconvolution of the C 1s spectrum (Fig. 3b). The six components of the C 1s spectrum can be assigned as follows: the lowest binding energy component at 284.6 eV which contributes with 26.3% to the total C 1s intensity is assigned to C–C and C–H bonds, while the one at 285.5 eV (38.1%) is due to C–O and C–N bonds. Additionally, the peak at 286.6 eV (18.1%) is attributed to the C–O–C group and the one at 287.8 eV (7.6%) originates from C═O and C═N groups. The component at 288.8 eV (7.3%) corresponds to C(O)O groups, whereas the highest binding energy component at 289.7 eV (2.6%) is associated with π–π shake-up features.[25,32]

The optical properties of the NCNDs-Lap suspensions were studied by means of UV-Vis optical absorption and photoluminescence emission (PL) and excitation (PLE) spectroscopy and were found to be similar to the NCNDs in solution,[25] thus confirming that the Lap matrix did not perturb the photophysical properties of the embedded NCNDs. The UV-Vis spectrum (Fig. 4a) demonstrates the characteristic features of NCNDs, *i.e.* it exhibits gradual absorption from lower to higher energies and mainly below 400 nm while it displays a clear absorption band at ~290 nm which is correlated with the π–π* transition of the conjugated C═C units.[25]

The PL spectra (Fig. 4b) reveal the excitation-dependent luminescence behavior of the hybrid material as well as NCND solution. A clear red shift of the emission peaks from ~353 nm to ~518 nm is observed when increasing the excitation wavelength from 280 to 440 nm. The spectra display broad and multiple emissions as more clearly visible at higher excitation energies. For instance, with excitation at 280 nm, the spectrum presents a broad emission peak centered at ~353 nm and an even broader shoulder around 450 nm. The spectrum excited at 300 nm shows analogous features with its main emission at 360 nm and a broad emission in the visible region above ~420 nm for which the exact band position is difficult to define. 300 nm is also the optimal excitation wavelength for obtaining the maximum fluorescence intensity from the NCNDs-Lap suspension. The other spectra are similar and display descending luminescence intensity as the emission is

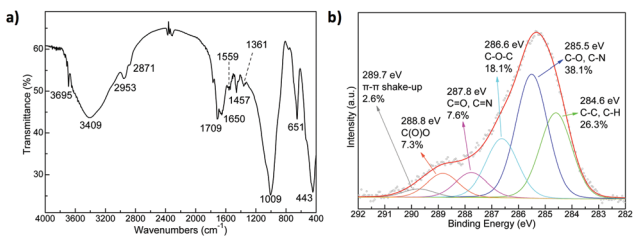

Fig. 3 (a) FT-IR spectrum and (b) C 1s core level photoemission spectrum of the NCNDs-Lap hybrid prepared with the top-down approach.

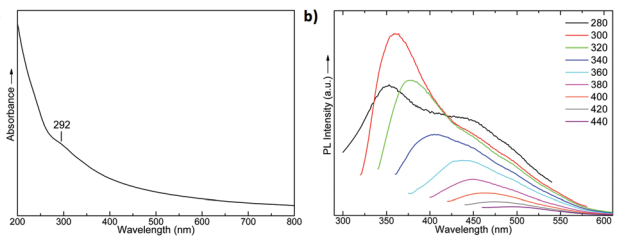

Fig. 4 (a) UV-Vis absorption spectrum and (b) photoluminescence emission (PL) spectra of a NCNDs-Lap aqueous suspension.

broadened and red shifted. The multiple emission bands as well as the shift to lower energies upon excitation with ascending wavelengths clearly suggest the presence of various and diverse emissive states. These originate from the several existing surface groups and traps, a fact that explicates the complicated excitation-dependence of the PL spectra along with the size-dependence.[25]

Furthermore, comparison of the PL spectra suggests that there should be at least one main absorptive band below 300 nm, in agreement with the UV-Vis spectrum, and alternative deactivation pathways that give rise to further emission peaks. The high energy absorption is linked with the π–π* transitions of C=C units, whereas the lower energy absorptions correspond to n–π* transitions. Nitrogen doping causes a blue shift, while introduction of oxygen atoms containing functional groups induces more electronic states between the NCNDs' π–π* bandgap guiding to a red shift in the observed PL. The additional states originate either by n electrons from C=O units near the π band or by introduced energy levels from C–O and C–O–C groups just below the π* band.[9,25,33,34] Hence, the spectral features of the PL spectra are clarified as follows: when NCNDs-Lap is excited with high energy (280 nm) capable of inducing π–π* transitions, a relatively high energy deactivation band dominates the spectrum (353 nm), while alternative deactivation pathways linked with n–π* transitions are also present (shoulder at ~450 nm). In contrast, with lower energy excitation (300 nm and longer), the n–π* transitions become predominant and various recombination pathways occur, thus explaining also the broadening of the emissions which is better observed for the spectra with excitation at ≥340 nm.

The PLE spectra (Fig. S5†) confirm the interpretation of the UV-Vis and PL spectra as far as the presence of multiple absorptive bands and deactivation pathways is concerned. Locking emission at 380 nm, a broad excitation band centered at ~300 nm and a higher energy peak at ~245 nm are observed. This agrees with the band at 292 nm and the rapid increase in absorption below ~250 nm in the UV-Vis spectrum. In fact, this further supports the photoluminescence findings (PL spectrum, $\lambda_{exc.}$ at 300 nm), where the maximum luminescence of the NCNDs-Lap hybrid results when exciting at 300 nm with broad emission centered at 360 nm and thus significant fluorescence intensity at 380 nm (PLE spectrum, $\lambda_{em.}$ at 380 nm). The second PLE spectrum with $\lambda_{em.}$ at 450 nm displays two excitation bands; one near 280 nm and another at ~375 nm, in agreement with the PL spectra ($\lambda_{exc.}$ at 280 and 380 nm) where emission at ~450 nm is observed, and with the UV-Vis spectrum where in addition to the ~290 nm band, a slight shoulder around 350 nm seems to exist. Overall, the presented PL/PLE spectra converge to the conclusion that there are various electronic states within the NCNDs' bandgap (π–π*) as reported in the literature on CNDs.[9,25,30,31]

Bottom-up approach

The bottom-up LbL approach presents the advantage over the typical solution chemistry in that it allows the precise control

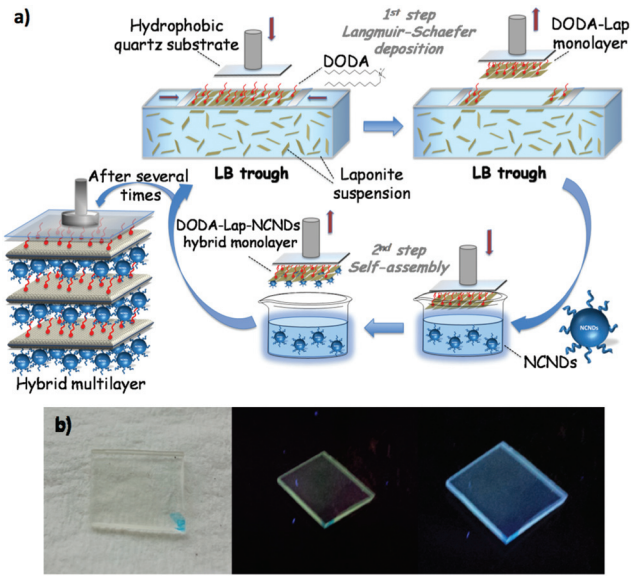

Fig. 5 (a) Schematic representation of the deposition cycle for the DODA-Lap-NCND multilayer film. Transfer of the DODA-clay monolayer onto a substrate in the first step, followed by the grafting of NCNDs onto the DODA-clay monolayer. This cycle could be repeated as many times as required; (b) digital photographs of the hybrid transparent DODA-Lap-NCND multilayer film (80 layers) deposited on quartz in daylight (left), under UV (254 nm) illumination (center) and UV (365 nm) illumination (right).

of the number of layers and layering sequence during the film formation, which translates to a higher degree of ordering,[35,36] as also observed for the LAPONITE®-carbon dot film we discuss here.

As illustrated in Fig. 5a and described in detail in the Experimental section, in the first step a dimethyldioctadecylammonium (DODA)-Lap monolayer was prepared at the air/water interface and attached onto a substrate. In the second step, the DODA-Lap layer was dipped into a solution of NCNDs for self-assembly, resulting in a luminescent DODA-Lap-NCND multilayer film (Fig. 5b). The repetition of this nanofabrication cycle could finally result in well-controlled structures with the desired number of NCND layers.

As shown in Fig. 6a, the XRD pattern of the as-prepared DODA-Lap-NCND film displays a 001 peak which is significantly narrower compared to that of NCNDs-Lap (Fig. 2a) and that of pristine Lap. This narrow 001 peak results from the higher number of the stacking clay layers and also suggests a better orientation among the layers than in NCNDs-Lap or pristine Lap.

In addition, the *d*-spacing, calculated to be 25.7 ± 0.3 Å, corresponds to a considerably larger interlamellar space, namely ~16 Å, than calculated for the NCNDs-Lap hybrid prepared in bulk, due to the presence of DODA in the clay interlayer. In addition, we cannot exclude that bigger NCNDs may have been intercalated between the LAPONITE® layers as the effective space is larger. In fact, during the self-assembly process, NCNDs attach to the surface and may penetrate

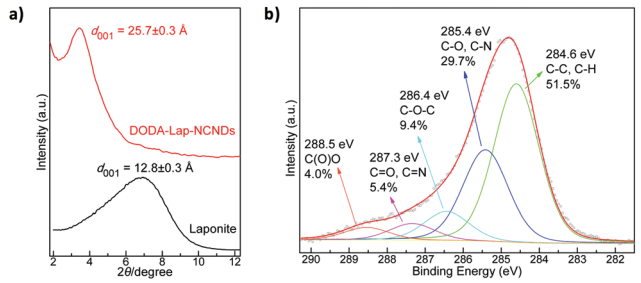

Fig. 6 (a) X-ray powder diffraction patterns of LAPONITE® and of a DODA-Lap-NCND multilayer film (80 layers); (b) C 1s core level photoemission spectrum of a DODA-Lap-NCND multilayer film (80 layers).

among the easily movable DODA tails so that NCNDs of a maximum diameter of ~15 Å can be hosted in the hybrid structure.

XPS was also employed for the surface analysis of the DODA-Lap-NCND films (Fig. 6b). Once more, carbon, nitrogen, oxygen, silicon and magnesium were detected in survey spectra (not shown), while fitting the C 1s spectrum results in five major contributions. The peak at 284.6 eV which contributes with 51.5% to the total C 1s intensity derives from C–C and C–H bonds. This is much larger in the LbL film than in the bulk synthesized hybrid because of the presence of DODA. 29.7% of the total C 1s intensity is due to C–O and C–N bonds giving rise to a peak centered at 285.4 eV and the peak derived from C–O–C groups at 286.4 eV contributes 9.4%. The small contributions at 287.3 eV band (5.4%) and at 288.5 eV (4.0%) are assigned to C═O/C═N groups and C(O)O groups, respectively.

The LbL films were further characterized by UV-Vis and PL/PLE spectroscopy methods (Fig. 7). The absorption spectrum of the produced multilayer is identical to that of the drop-cast film (Fig. 4), exhibiting the same shoulder at ~290 nm. The transparency is controlled by the number of LbL self-assembly steps and consequently the number of layers; a 40-layer film is 85% transparent at 550 nm, while for the 80-layer film this value drops to 63%.

Extended PL spectra of the LbL films are shown in Fig. S3,† whereas for clarity reasons only the regions of the main peaks are presented here. Thus, as clearly observed, the LbL

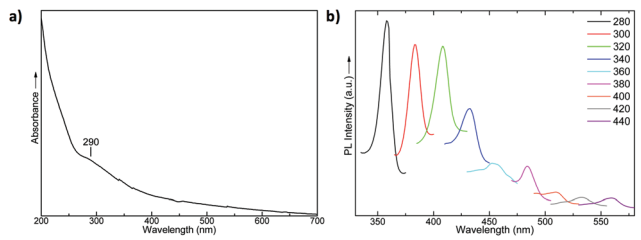

Fig. 7 (a) UV-Vis absorption spectrum and (b) photoluminescence emission (PL) spectra of a DODA-Lap-NCND multilayer film on quartz (80 layers).

films exhibit excitation-dependent luminescence behavior. Consequently, as the excitation wavelength increases from 280 to 440 nm, the dominant emission band is red shifted accordingly from 358 to 560 nm. The maximum luminescence intensity is observed when excitation at 280 nm occurs, whereas interpretation of the spectral characteristics connects the recorded fluorescence with both π–π* and n–π* transitions and varied deactivation pathways. The latter is better seen in Fig. S3† where additional – to the main peaks – emission bands are observed. As in the case of NCND-Lap suspensions, this is more obvious for spectra with high energy excitation wavelengths (280–320 nm) with the recombination pathways giving rise to emissions mainly in the ~450–470 nm region, in relevance with the shoulder at ~450 nm of NCNDs-Lap (Fig. 4, $\lambda_{exc.}$: 280 nm). On the other hand, compared to the PL spectra of NCND-Lap the spectra of DODA-Lap-NCND films exhibit narrower main emission peaks suggesting no water or interparticle interference and possible passivation by the DODA alkyl chains or in contrast a change in the emissive sites on the surface probably due to an interaction with DODA alkyl chains. Nevertheless, in general, the formed ultra-thin LbL films demonstrate analogous fluorescence and optoelectronic properties with the bulk NCNDs-Lap suspensions and succeeding drop-cast films.

This is further verified from the obtained PLE spectra of the DODA-Lap-NCND film (Fig. S6†). Three excitation bands at ~245, ~280 and ~375 nm are exposed when emission is locked either at 410 or at 460 nm; these are identical to those reported for bulk NCND-Lap suspensions (Fig. S5†). Hence, as discussed in detail for the NCNDs-Lap hybrid, it is also valid that the PLE spectra of the LbL DODA-Lap-NCND films are in accordance with the rest of the optical spectra (UV-Vis and PL) and the NCND optical properties are still strong and present in the multilayer film.

Conclusions

In summary, we successfully report a simple and novel preparation of nitrogen-doped carbon nanodot (NCND)-clay hybrids *via* two different approaches: bulk solution chemistry and layer-by-layer deposition realized by combining the Langmuir–Schaefer technique with self-assembly. In both cases, hybrids with intercalated NCNDs in the interlayer of LAPONITE® sheets are obtained, and a high NCND content (above 20 wt%) is achieved. In the hybrids, the NCNDs preserve their optoelectronic properties and exhibit excitation-dependent luminescence. In other words, the inert matrix of Lap protects the embedded NCNDs from external agents that could affect their optoelectronic properties. Furthermore, the transparency of the films can be tuned either by adjusting the dot concentration in the suspension used for the preparation of drop-cast films, or by controlling the number of layers in the films prepared by layer-by-layer deposition. Therefore, we demonstrate that stable and homogeneous hybrid materials, which may drive potential applications in optoelectronics, energy, cataly-

sis and biomedicine, can be prepared through the proper use of well-established approaches.

Acknowledgements

F. Arcudi and Prof. M. Prato acknowledge the University of Trieste, Consorzio Interuniversitario Nazionale per la Scienza e Tecnologia dei Materiali (INSTM), Ministero dell'Università e della Ricerca (MIUR) (FIRB prot. RBAP11C58Y and Cofin. Prot. 2010N3T9M4) and the European Commission (FP7/2007–2013 under grant agreement number 310651, SACS project) for financial support. A. K. acknowledges the Ubbo Emmius Program for a PhD fellowship.

References

1 Y.-P. Sun, B. Zhou, Y. Lin, W. Wang, K. A. S. Fernando, P. Pathak, M. J. Meziani, B. A. Harruff, X. Wang, H. Wang, P. G. Luo, H. Yang, M. E. Kose, B. Chen, L. M. Veca and S.-Y. Xie, *J. Am. Chem. Soc.*, 2006, **128**, 7756–7757.
2 X. Xu, R. Ray, Y. Gu, H. J. Ploehn, L. Gearheart, K. Raker and W. A. Scrivens, *J. Am. Chem. Soc.*, 2004, **126**, 12736–12737.
3 S. N. Baker and G. A. Baker, *Angew. Chem., Int. Ed.*, 2010, **49**, 6726–6744.
4 Y. Wang and A. Hu, *J. Mater. Chem. C*, 2014, **2**, 6921–6939.
5 A. Zhao, Z. Chen, C. Zhao, N. Gao, J. Ren and X. Qu, *Carbon*, 2015, **85**, 309–327.
6 S. Y. Lim, W. Shen and Z. Gao, *Chem. Soc. Rev.*, 2015, **44**, 362–381.
7 J. Shen, Y. Zhu, X. Yang and C. Li, *Chem. Commun.*, 2012, **48**, 3686–3699.
8 X. Li, M. Rui, J. Song, Z. Shen and H. Zeng, *Adv. Funct. Mater.*, 2015, **25**, 4929–4947.
9 K. Dimos, *Curr. Org. Chem.*, 2016, **20**, 682–695.
10 C. Ding, A. Zhu and Y. Tian, *Acc. Chem. Res.*, 2014, **47**, 20–30.
11 S. Carrara, F. Arcudi, M. Prato and L. De Cola, *Angew. Chem., Int. Ed.*, 2017, **56**, 4757–4761.
12 F. Arcudi, L. Đorđević and M. Prato, *Angew. Chem., Int. Ed.*, 2017, **56**, 4170–4173.
13 X. Zou and B. I. Yakobson, *Acc. Chem. Res.*, 2015, **48**, 73–80.
14 H. Tetsuka, T. Ebina and F. Mizukami, *Adv. Mater.*, 2008, **20**, 3039–3043.
15 L. Jankovic, K. Dimos, J. Bujdak, I. Koutselas, J. Madejova, D. Gournis, M. A. Karakassides and P. Komadel, *Phys. Chem. Chem. Phys.*, 2010, **12**, 14236–14244.
16 H. Tetsuka, A. Nagoya and R. Asahi, *J. Mater. Chem. C*, 2015, **3**, 3536–3541.
17 M. Zhang, Q. Yao, W. Guan, C. Lu and J.-M. Lin, *J. Phys. Chem. C*, 2014, **118**, 10441–10447.
18 A. Vassilakopoulou, V. Georgakilas, N. Vainos and I. Koutselas, *J. Phys. Chem. Solids*, 2017, **103**, 190–196.
19 A. Vassilakopoulou, V. Georgakilas and I. Koutselas, *J. Sol-Gel Sci. Technol.*, 2017, **82**, 795–800.
20 A. Kovalchuk, K. Huang, C. Xiang, A. A. Martí and J. M. Tour, *ACS Appl. Mater. Interfaces*, 2015, **7**, 26063–26068.
21 S. K. Bhunia, S. Nandi, R. Shikler and R. Jelinek, *Nanoscale*, 2016, **8**, 3400–3406.
22 Y.-F. Huang, X. Zhou, R. Zhou, H. Zhang, K.-B. Kang, M. Zhao, Y. Peng, Q. Wang, H.-L. Zhang and W.-Y. Qiu, *Chem. – Eur. J.*, 2014, **20**, 5640–5648.
23 K. Jiang, S. Sun, L. Zhang, Y. Lu, A. Wu, C. Cai and H. Lin, *Angew. Chem., Int. Ed.*, 2015, **54**, 5360–5363.
24 H. H. Murray, *Appl. Clay Sci.*, 1991, **5**, 379–395.
25 F. Arcudi, L. Đorđević and M. Prato, *Angew. Chem., Int. Ed.*, 2016, **55**, 2107–2112.
26 L. M. Toma, R. Y. N. Gengler, E. B. Prinsen, D. Gournis and P. A. Rudolf, *Phys. Chem. Chem. Phys.*, 2010, **12**, 12188–12197.
27 A. Michopoulos, A. Kouloumpis, D. Gournis and M. I. Prodromidis, *Electrochim. Acta*, 2014, **146**, 477–484.
28 A. Kouloumpis, K. Spyrou, K. Dimos, V. Georgakilas, P. Rudolf and D. Gournis, *Front. Mater.*, 2015, **2**, 10.
29 E. Giannakopoulos, P. Stathi, K. Dimos, D. Gournis, Y. Sanakis and Y. Deligiannakis, *Langmuir*, 2006, **22**, 6863–6873.
30 B. K. G. Theng, *The Chemistry of Clay-Organic Reactions*, Adam Hilger, London, UK, 1974.
31 M. Jaber and J.-F. Lambert, *J. Phys. Chem. Lett.*, 2010, **1**, 85–88.
32 N. Liaros, J. Tucek, K. Dimos, A. Bakandritsos, K. S. Andrikopoulos, D. Gournis, R. Zboril and S. Couris, *Nanoscale*, 2016, **8**, 2908–2917.
33 S. Hu, A. Trinchi, P. Atkin and I. Cole, *Angew. Chem., Int. Ed.*, 2015, **54**, 2970–2974.
34 V. Strauss, J. T. Margraf, C. Dolle, B. Butz, T. J. Nacken, J. Walter, W. Bauer, W. Peukert, E. Spiecker, T. Clark and D. M. Guldi, *J. Am. Chem. Soc.*, 2014, **136**, 17308–17316.
35 K. Ariga, Y. Yamauchi, T. Mori and J. P. Hill, *Adv. Mater.*, 2013, **25**, 6477–6512.
36 P. Lavalle, J.-C. Voegel, D. Vautier, B. Senger, P. Schaaf and V. Ball, *Adv. Mater.*, 2011, **23**, 1191–1221.

